Revised for Submission to Soft Matter (March 2020)

Supporting Information

for

Dispersing nano- and micro-sized portlandite particulates via electrosteric exclusion at short screening lengths

*Jason Timmons ([a,b,+]), Iman Mehdipour ([b,+]), Shang Gao ([c]), Hakan Atahan ([b,d]), Narayanan Neithalath ([e]), Mathieu Bauchy ([f,i]), Edward Garboczi ([g]), Samanvaya Srivastava ([c,i,**]), Gaurav Sant ([a, b,h,i,**])*

[a] Department of Materials Science and Engineering, University of California, Los Angeles, CA 90095, USA
[b] Laboratory for the Chemistry of Construction Materials (LC^2), Department of Civil and Environmental Engineering, University of California, Los Angeles, CA 90095, USA
[c] Department of Chemical and Biomolecular Engineering, University of California, Los Angeles, CA 90095, USA
[d] Department of Civil Engineering, Istanbul Technical University, Istanbul, Turkey
[e] School of Sustainable Engineering and the Built Environment, Arizona State University, Tempe, AZ 86587, USA
[f] Laboratory for the Physics of Amorphous and Inorganic Solids (PARISlab), Department of Civil and Environmental Engineering, University of California, Los Angeles, CA 90095, USA
[g] Applied Chemicals and Materials Division, Material Measurement Laboratory, National Institute of Standards and Technology, Boulder, CO 80305, USA
[h] California Nanosystems Institute (CNSI), University of California, Los Angeles, CA 90095, USA
[i] Institute for Carbon Management, University of California, Los Angeles, CA 90095, USA

[+] Both authors contributed equally to this work.

[**]Corresponding authors: S. Srivastava, Email: samsri@ucla.edu and G. Sant, Email: gsant@ucla.edu

Number of pages: 6 (including the title page)
Number of figures: 5

(A) Particle Size Distribution

The particle size distribution of portlandite particulates was determined by static light scattering. To confirm that the particle size distribution measured by this technique was that of aggregates of particles, SEM and TEM were performed (see Figure S1).

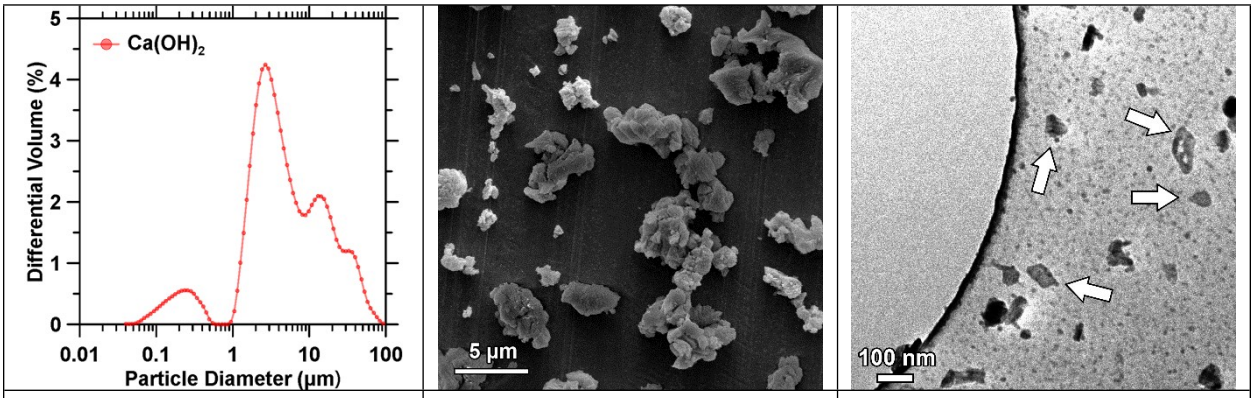

Figure S1: (a) The particle size distribution of portlandite particulates as determined by static light scattering (SLS), revealing a volumetric median diameter, d_{50} = 3.8 µm. **(b)** SEM micrograph displaying the morphology of portlandite particle aggregates. **(c)** A TEM micrograph of portlandite particulates with primary particles indicated by the arrows.

(B) Fourier Transform Infrared Spectroscopy

Fourier Transform Infrared (FTIR, PerkinElmer Spectrum Two)* spectroscopy was performed on each of the three dispersants. From the spectra, shown in Figure S2, three relevant functional groups have been identified: the carbonyl group, present on the PAA backbone, the ether group, present on the side chains in PCE, and the sulfonic acid group, present in LS but also appearing slightly in PAA.

* Certain commercial equipment, software and/or materials are identified in this paper in order to adequately specify the experimental procedure. In no case does such identification imply recommendation or endorsement by the National Institute of Standards and Technology, nor does it imply that the equipment and/or materials used are necessarily the best available for the purpose.

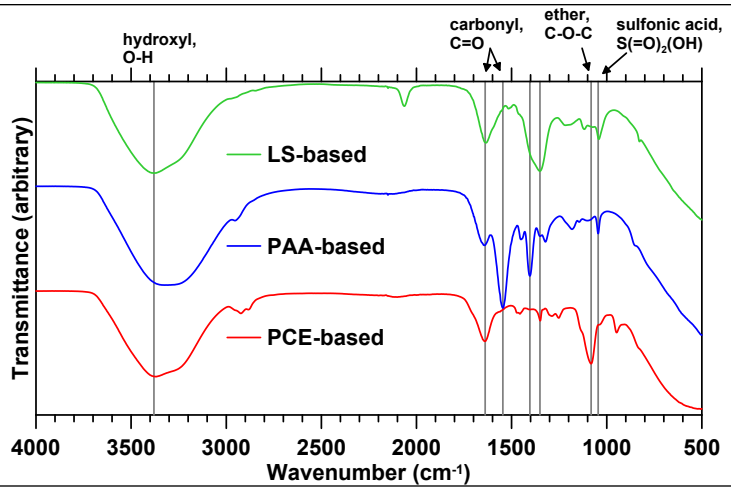

Figure S2: Determination of select functional groups present on each dispersant.

(C) Lifshitz Theory for Calculation of the Hamaker Constant

The following equation was used to calculate the Hamaker Constant A for the suspension of the $Ca(OH)_2$ particles (denoted by subscript p) and saturated $Ca(OH)_2$ solutions (denoted by subscript m). It includes terms for the Boltzmann constant (k_b), permittivity (ε), refractive index (n), Planck constant (h), and electron frequency (ν_e).[1]

$$A = \frac{3}{4}kT\left(\frac{\varepsilon_p - \varepsilon_m}{\varepsilon_p + \varepsilon_m}\right)^2 + \frac{3h\nu_e}{16\sqrt{2}}\frac{\left(n_p^2 - n_m^2\right)^2}{\left(n_p^2 + n_m^2\right)^{3/2}}$$ **Equation S1**

(D) Kinetic Stability Criterion

This methodology follows that of Israelachvili.[1] A suspended particle (mass m_p, diameter D, density ρ_p) has a velocity v due to thermal (Brownian) forces caused by random motion of the solvent, with kinetic energy on the order of the thermal energy, approximately the product of the Boltzmann constant k and the absolute temperature T:

$$\frac{1}{2}m_p v^2 = \frac{1}{2}\left[\frac{4}{3}\pi\left(\frac{D}{2}\right)^3\rho_p\right]v^2 \approx kT$$ **Equation S2**

The average particle velocity can thus be determined as:

$$v \approx \sqrt{\frac{12kT}{\pi d^3 \rho_p}}$$ **Equation S3**

The number density of particles N_p is given by the ratio of the total mass of particles m_{pT} over the mass of a single particle m_p. The total mass of particles can be determined from the particle concentration c and the medium density ρ_m.

$$N_p = \frac{m_{pT}}{m_p} = \frac{c\rho_m}{\frac{4}{3}\pi\left(\frac{D}{2}\right)^3\rho_p}$$ **Equation S4**

The cubic root of the number density gives the linear number density of particles, the inverse of which gives the distance between particles – the interparticle spacing *d*.

$$d = \frac{1}{\sqrt[3]{N_p}} \qquad \textbf{Equation S5}$$

The collision frequency f_c is given by the inverse of the time it takes a particle to travel the interparticle distance:

$$f_c = \frac{v}{d} \qquad \textbf{Equation S6}$$

The probability *p* of two particles having sufficient energy to overcome a repulsive barrier *E*:

$$p = \exp\left(\frac{-E}{kT}\right) \qquad \textbf{Equation S7}$$

For a given time *t*, one can then determine the minimum barrier for which no collisions are energetic enough to overcome this barrier:

$$\left(\frac{E}{kT}\right)_{min} = \ln\left(tf_c\right) \qquad \textbf{Equation S8}$$

This value is dependent on particle size; for 24 h of stability: 20 nm -> 28 kT, 100 nm -> 25 kT, 200 nm -> 22 kT

(E) Yield stress Behavior for PCE-containing Suspensions

Figure S3 shows yield stress results determined at a variety of solid volume fractions and PCE dosages, following the same procedure described in the main body of the paper. It illustrates that the impact of PCE is systematic across the range of yield stresses and solid volume fractions examined here, and that higher solid volume fractions are accessible due to increasing the dosage of PCE.

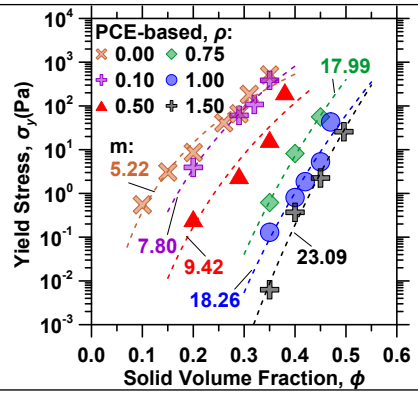

Figure S3: Yield stress-particle volume fraction curves of $Ca(OH)_2$ suspensions at varying PCE dosages. Data was fitted by a power-law function of the form $\sigma_y = a(\phi)^m$.

(F) Fractal Dimension of Aggregates

The fractal dimension D_f of suspensions composed at varying dispersant dosages was calculated from the data and fits presented in Figure S3. These results are reported in the main text, Figure 2b. The data was fit to an expression of the form $\sigma_y = a(\phi)^m$, where $m = \frac{D+X}{D-D_f}$, D being the number of spatial dimensions (3) and X as the fractal dimension of the cluster backbones, taken as 1.[2] Each fit was determined for a series of suspensions at varying solid volume fractions for each dispersant dosage. For PCE, the range of volume fractions was gradually increased along with the dosage, to illustrate the increase of maximum solid volume.

(G) Crossover Energy

The crossover energy of select suspensions at a fixed volume fraction (ϕ = 0.25) was determined. The crossover energy is defined as the integral of the storage modulus (G') from 0.001 strain amplitude (γ) to the crossover point (γ_{cr}), where the loss modulus (G'') first exceeds the storage modulus. Thus, the work required to break down the structure of suspension can be expressed as $E_{cr} = \int_{0.001}^{\gamma_{cr}} \gamma_{cr} G' d\gamma$. Figure S4a illustrates the method of calculating the crossover energy, and Figure S4b shows the trends with dosage, which follows that of yield stress very closely. The crossover energy describes the strength of aggregates, as it is the energy required to alter the suspension from a solid-like state (low strain amplitude, high storage modulus) to a liquid-like state (high strain amplitude, $G'' > G'$). Suspensions containing PCE have the lowest crossover energy, signifying that any aggregates present are significantly weaker than those found in suspensions with other dispersants or no dispersant.

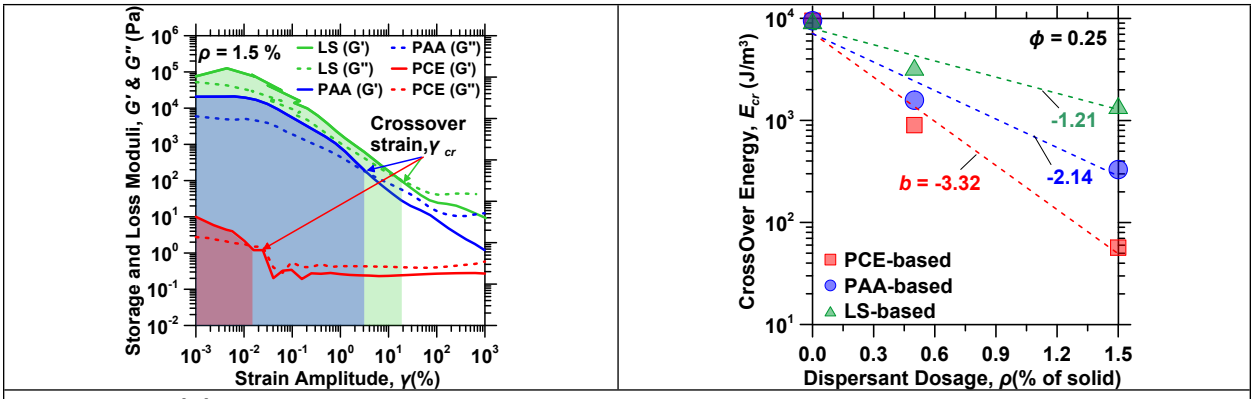

Figure S4: (a) Representative illustration of the method of calculating crossover energy for two examples of suspensions. **(b)** The dependence of crossover energy of $Ca(OH)_2$ suspensions to dispersant type for varying dispersant dosages. The dashed lines indicate exponential function fits to the data of the form $\sigma_y = a\exp(-b\rho)$, where a and b are fitting parameters and ρ is the dispersant dosage.

(H) Nuclear Magnetic Resonance Characterization

To obtain information about the structure of each polymer, proton nuclear magnetic resonance spectroscopy (^{1}H NMR; Bruker AV400) was performed. The carrier fluid for each polymer was deuterium oxide (D_2O); as each dispersant is provided in aqueous solution, they were first dried via a combination of vacuum desiccation and oven drying at 60 °C. 10 mg of the dry polymer was then added to D_2O and dissolved with the aid of ultrasonication, and then further analyzed. The structure of PCE (Figure S5) was determined from these results and it was found that the backbone unit (*m*) to side chain unit (*n*) for each group was 1:1. Due to unreacted PEG side chains present in samples, the correct proportion of a number of PEG units in the side chain (*p*) could not be determined directly from NMR. This proportion was instead inferred from the relative peaks for the groups determined from FTIR (*p* = 18), as described elsewhere.[3] Combining these results with the known total molecular weight (i.e., backbone + side chain), a number of backbone units and side chain units were found to be *m* = *n* = 41.

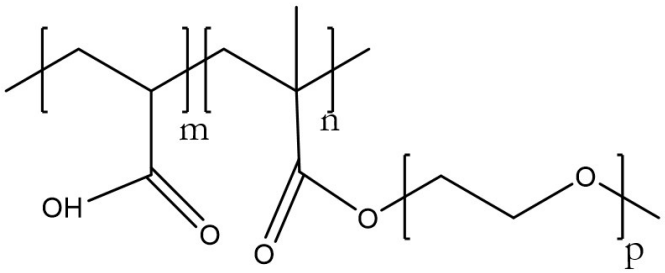

Figure S5: The estimated structure of the PCE-based dispersant.

References

1 J. N. Israelachvili, *Intermolecular and Surface Forces*, Academic Press, 2015.
2 W.-H. Shih, W. Y. Shih, S.-I. Kim, J. Liu and I. A. Aksay, *Phys. Rev. A*, 1990, **42**, 4772–4779.
3 L. M. Rueschhoff, J. P. Youngblood and R. W. Trice, *J. Am. Ceram. Soc.*, 2016, **99**, 3857–3865.